Kinetic and Structural Insight into the Mechanism of BphD, a C−C Bond Hydrolase from the Biphenyl Degradation Pathway†

Geoff P. Horsman,[‡,||] Jiyuan Ke,[§,||,⊥] Shaodong Dai,[§,#] Stephen Y. K. Seah,[‡,▽] Jeffrey T. Bolin,[§] and Lindsay D. Eltis*[,‡]

Departments of Biochemistry and Molecular Biology, and Microbiology and Immunology, University of British Columbia, Vancouver, BC V6T 1Z3, Canada, and Purdue Cancer Center and Markey Center for Structural Biology, Department of Biological Sciences, Purdue University, West Lafayette, Indiana 47907-2054

Received June 5, 2006; Revised Manuscript Received July 10, 2006

ABSTRACT: Kinetic and structural analyses of 2-hydroxy-6-oxo-6-phenylhexa-2,4-dienoic acid (HOPDA) hydrolase from *Burkholderia xenovorans* LB400 ($BphD_{LB400}$) provide insight into the catalytic mechanism of this unusual serine hydrolase. Single turnover stopped-flow analysis at 25 °C showed that the enzyme rapidly ($1/\tau_1 \sim 500\ s^{-1}$) transforms HOPDA ($\lambda_{max} = 434$ nm) into a species with electronic absorption maxima at 473 and 492 nm. The absorbance of this enzyme-bound species (E:S) decayed in a biphasic manner ($1/\tau_2 = 54\ s^{-1}$, $1/\tau_3 = 6\ s^{-1} \sim k_{cat}$) with simultaneous biphasic appearance (48 and 8 s^{-1}) of an absorbance band at 270 nm characteristic of one of the products, 2-hydroxypenta-2,4-dienoic acid (HPD). Increasing solution viscosity with glycerol slowed $1/\tau_1$ and $1/\tau_2$ but affected neither $1/\tau_3$ nor k_{cat}, suggesting that $1/\tau_2$ may reflect diffusive HPD dissociation, and $1/\tau_3$ represents an intramolecular event. Product inhibition studies suggested that the other product, benzoate, is released after HPD. Contrary to studies in a related hydrolase, we found no evidence that ketonized HOPDA is partially released prior to hydrolysis, and, therefore, postulate that the biphasic kinetics reflect one of two mechanisms, pending assignment of E:S ($\lambda_{max} = 492$ nm). The crystal structures of the wild type, the S112C variant, and S112C incubated with HOPDA were each determined to 1.6 Å resolution. The latter reveals interactions between conserved active site residues and the dienoate moiety of the substrate. Most notably, the catalytic residue His265 is hydrogen-bonded to the 2-hydroxy/oxo substituent of HOPDA, consistent with a role in catalyzing ketonization. The data are more consistent with an acyl−enzyme mechanism than with the formation of a *gem*-diol intermediate.

The microbial degradation of aromatic compounds is crucial to maintaining the global carbon cycle (*1*). Aerobic degradation typically involves oxygenation of the aromatic ring to produce a catechol followed by a dioxygenase-catalyzed ring-opening reaction. In one type of degradation pathway, ring-opening yields a meta-cleavage product (MCP[1]). A serine hydrolase then catalyzes carbon−carbon bond hydrolysis of the MCP, generating 2-hydroxypenta-2,4-dienoic acid (HPD). This strategy is utilized in the Bph pathway responsible for the degradation of biphenyl (Figure 1). HPD is further transformed to pyruvic acid for the TCA cycle, thereby allowing microorganisms to grow on aromatic compounds (*2*). The MCP hydrolases are, therefore, important catabolic enzymes.

MCP hydrolases are of interest to the fields of biodegradation and pathogenesis. First, like other degradation enzymes, they are able to transform the metabolites of some xenobiotic compounds. One important example is the degradation of the metabolites of polychlorinated biphenyls (PCBs) within the Bph pathway. In this case, overall degradation of PCBs may be limited in part by the poor turnover of certain chlorinated 2-hydroxy-6-oxo-6-phenylhexa-2,4-dienoic acids (HOPDAs) by the HOPDA hydrolase, BphD (*3*). Thus, structure−function studies of BphD should advance protein engineering efforts to improve its activity toward chlorinated substrates, facilitating the biodegradation of PCBs (*2*, *4*). With respect to pathogenesis, a close homologue of BphD was recently found to be critical for the survival of *Mycobacterium tuberculosis* in the macrophage (*5*). The mycobacterial homologue catalyzes HOPDA hydrolysis (*6*) and appears to be involved in cholesterol degradation (Van der Geize et al., unpublished results). Greater understanding of BphD and its inhibitors could, thus, be useful to develop novel therapeutics for tuberculosis.

† This work was funded by the Natural Sciences and Engineering Research Council of Canada (Discovery Grant) and the National Institutes of Health (GM-52381).

* Corresponding author. Phone: (604) 822-0042. Fax: (604)822-6041. E-mail: leltis@interchange.ubc.ca.

‡ University of British Columbia.

§ Purdue University.

|| These authors contributed equally to this work.

⊥ Present address: University of Kentucky, Lexington, KY 40506.

Present address: Howard Hughes Medical Institute, National Jewish Medical and Research Center, Denver, CO 80206.

▽ Present address: Department of Molecular and Cellular Biology, University of Guelph, Guelph, ON N1G 2W1, Canada.

[1] Abbreviations: MCP, meta-cleavage product; HPD, 2-hydroxypenta-2,4-dienoic acid; PCB, polychlorinated biphenyl; HOPDA, 2-hydroxy-6-oxo-6-phenylhexa-2,4-dienoic acid; DHB, 2,3-dihydroxybiphenyl; DHBD, dihydroxybiphenyl dioxygenase; S^k, ketonized substrate; $E:S^k$, enzyme-bound ketonized substrate; P, polar; NP, nonpolar; *I*, ionic strength.

10.1021/bi0611098 CCC: $33.50 © 2006 American Chemical Society
Published on Web 08/26/2006

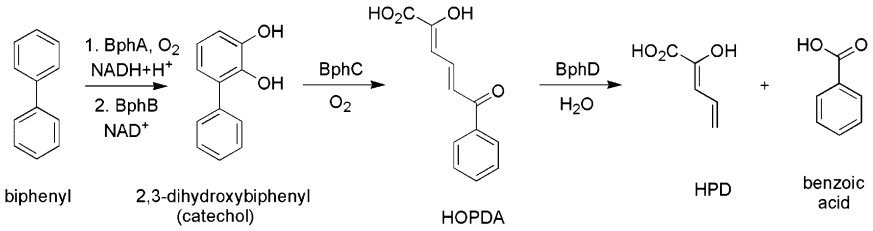

FIGURE 1: The aerobic microbial degradation of biphenyl by the upper Bph pathway is typical of aromatic compound degradation via the meta-cleavage pathway. The meta-cleavage product, HOPDA, is hydrolyzed in an unusual reaction by the final enzyme, BphD.

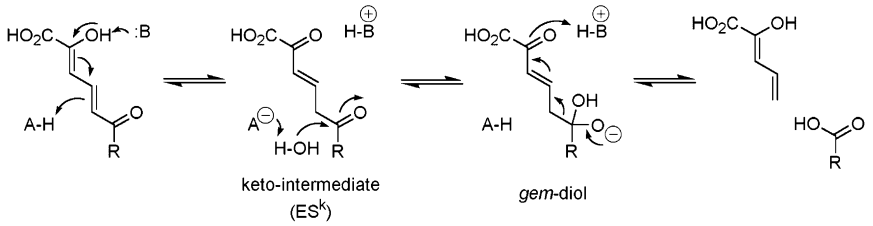

FIGURE 2: Proposed enol−keto tautomerization and subsequent hydrolytic C−C cleavage catalyzed by the MCP hydrolases.

BphD from *Burkholderia xenovorans* LB400 ($BphD_{LB400}$), a potent PCB-degrader, exemplifies MCP hydrolases, catalyzing the unusual cleavage of a carbon−carbon bond (Figure 1). It is a member of the α/β-hydrolase superfamily (*7*−*9*) and contains conserved Ser-His-Asp residues that might be expected to constitute a catalytic triad, enabling the acyl−enzyme mechanism common to many well-characterized hydrolytic enzymes. In this mechanism, the hydrogen-bonding network between the triad of conserved residues serves to activate the serine hydroxyl for nucleophilic attack at the carbonyl carbon of the scissile bond. Expulsion of the leaving group results in acylated serine, which is then deacylated by histidine-mediated hydrolysis. However, it is unlikely that BphD and other MCP hydrolases follow this exact mechanism. For example, many hydrolases attack substrates endowed with electron sinks, such as alcohols (esterases and lipases), amines (proteases), and α-ketones (β-ketolases); protonation of these entities provides good leaving groups. In contrast, the substrates for MCP hydrolases apparently have no such electron sink available upon carbon−carbon bond cleavage but rather have an electron-rich dienoate. Therefore, Bugg and colleagues proposed a two-phase mechanism that includes a preliminary enol−keto tautomerization to generate an electron sink prior to hydrolysis (Figure 2) (*10*). This requires additional catalytic residues to participate in acid−base chemistry or an alternative use of the triad residues to generate the keto-intermediate. In addition, they proposed that the catalytic serine serves as a base to activate water as the nucleophile, obviating the acyl-serine intermediate. Elucidating the mechanism of BphD is, therefore, of considerable interest.

Early mechanistic investigations advanced the idea of enol−keto tautomerization as a key feature of catalysis in MhpC, the MCP hydrolase in the phenylpropionic acid degradation pathway. Enzyme-catalyzed deuterium exchange at H-5 of the substrate provided indirect support for the existence of the keto-intermediate, and also suggested its partial release during the catalytic cycle (*11*). Stopped-flow kinetic analysis at acidic pH demonstrated a biphasic decay of the substrate, consistent with a rapid ketonization followed by slower hydrolysis. The stopped-flow data supported a model that included partial release of the keto-intermediate, which is consistent with the deuterium exchange results (*12*).

Experimental evidence favoring a *gem*-diol intermediate, rather than an acyl−enzyme mechanism, has been obtained in MhpC. Specifically, radiochemical trapping provided low stoichiometry of a covalent intermediate, ^{18}O was partially incorporated into both oxygen atoms of the carboxylic acid product, and ^{18}O was exchanged into the carbonyl of a nonhydrolyzable substrate analogue (*13*). In BphD, the processing of a reduced substrate required base catalysis (*14*), and the negative ρ value obtained from Hammett analysis is opposite in sign to values obtained for hydrolases using a nucleophilic serine mechanism (*14*, *15*). Overall, these results are more consistent with a mechanism involving the generation of a *gem*-diol intermediate formed via a base-catalyzed attack of water (Figure 2) (*16*) than a classical acyl−enzyme hydrolytic mechanism.

Crystal structures of four MCP hydrolases have been reported: $BphD_{RHA1}$ from *Rhodococcus sp*. strain RHA1 (*17*); $CumD_{IP01}$ from *Pseudomonas fluorescens* IP01, involved in cumene degradation (*18*); $CarC_{J3}$ from *Janthinobacterium sp*. strain J3, involved in carbazole degradation (*19*); and MhpC (*20*). All enzymes have an α/β-hydrolase fold with the conserved Ser, His, and Asp located between the core and lid domains. The structure of MhpC in complex with an inhibitor lacking the dienoate moiety has provided some insight into possible catalytic residues (*20*). Although two orientations of the inhibitor were observed in the active site, the orientation likely mimicking dienoate binding indicated that the C-1 carboxylate interacts with conserved Arg190 and Asn51 residues ($BphD_{LB400}$ numbering). The catalytic His was close to both the C-2 hydroxyl and C-5, implying that it may be involved in proton transfer between these positions during tautomerization. On the basis of the structural data and stopped-flow kinetic studies of MhpC mutants, the authors proposed that His265 catalyzes both the tautomerization and deprotonation of water for C−C cleavage, whereas Ser112 may stabilize the *gem*-diolate tetrahedral intermediate via hydrogen bonding (*21*). Different crystal forms of CumD show a shift in position of the His residue, lending support to this hypothesis (*18*). Although the MhpC

inhibitor complex advances our understanding of the catalytic mechanism of the MCP hydrolases, a complex with the unmodified dienoate moiety would more clearly delineate the catalytic roles of active site residues.

We investigated the catalytic mechanism of $BphD_{LB400}$ using steady-state and transient kinetic analyses together with structural analyses of the wild-type enzyme, a S112C variant, and a complex prepared by incubation of the latter with HOPDA. This study provides the first full spectra of catalytic intermediates for an MCP hydrolase. Further, it reveals key enzyme−substrate interactions, allowing us to predict the catalytic roles of active site residues.

MATERIALS AND METHODS

Chemicals. HOPDA was enzymatically generated from 2,3-dihydroxybiphenyl (DHB) using dihydroxybiphenyl dioxygenase (DHBD). Briefly, ~50 mg of DHB in 500 mL of buffer (potassium phosphate, $I = 100$ mM at pH 7.5) was quantitatively converted to HOPDA by DHBD. The HOPDA solution was acidified to pH 2 to 3 using 2 N HCl and extracted 3 times with 0.5 volumes of ethyl acetate. The organic extract was dried over anhydrous $MgSO_4$ and rotary evaporated to dryness. If necessary, the HOPDA was purified by HPLC from a methanol−water (0.5% H_3PO_4) mixture (80:20) using a Waters 2695 separation module fitted with a Prodigy 10-μm ODS-Prep column (21.2 × 250 mm) (Phenomenex, Torrance, CA). HOPDA was eluted in the same methanol/water (0.5% H_3PO_4) mixture at a flow rate of 7 mL/min. The HOPDA-containing fractions were pooled, extracted into ethyl acetate, dried, and evaporated as described above, yielding the purified HOPDA as a powder. 2,3-Dihydroxybiphenyl was prepared as previously described (*22*). Deuterium oxide was purchased from Cambridge Isotope Laboratories (Andover, MA), and protein sequencing grade trypsin and 3-methylcatechol from Aldrich (Mississauga, ON, Canada). All other chemicals were of analytical grade. Catechol 2,3-dioxygenase was used to prepare 2-hydroxy-6-oxo-2,4-heptadienoic acid from 3-methylcatechol as previously described (*23*).

Protein Production. $BphD_{LB400}$ and TodF (an MCP hydrolase from the toluene degradation pathway of *Pseudomonas putida* F1) were expressed and purified as previously described (*24*). The S112C variant of $BphD_{LB400}$ was expressed and purified as described for the wild-type enzyme. Selenomethionyl BphD was expressed in *E. coli* DL41 grown in minimal medium supplemented with selenomethionine (*25*). The active site serine of BphD was mutated to cysteine (S112C) using the transformer site-directed mutagenesis method (Clontech Laboratories, Palo Alto, CA). Briefly, the S112C mutagenic primer (primer S112C: 5′-GCGCCCCCCATGCAGTTGCCGACCAG-3′) and a second mutagenic selection primer to remove an *Eco*RI site (primer ODM: 5′-AGCTCGAATTGGTAATCATGG-3′) were mixed with the pEMBL18 plasmid containing the $BphD_{LB400}$ gene (pSS184) (*23*). After second strand synthesis and ligation using T4 DNA polymerase and T4 DNA ligase (Pharmacia, Uppsala, Sweden), respectively, the DNA was digested with *Eco*RI to linearize the unmutated plasmid and transformed into *E. coli* BMH 71-18 *mut*S. The plasmid isolated from this first transformation was subjected to a second round of *Eco*RI digestion and transformation, from which S112C mutants were isolated. The nucleotide sequence of the mutated gene was confirmed at the University of British Columbia DNA sequencing facility using an ABI 373 Stretch DNA sequencer (Applied Biosystems, Foster City, CA) and a BigDye v3.1 Terminator kit. The concentration of purified enzyme was determined using the molar absorptivity of $BphD_{LB400}$ ($\epsilon_{280} = 55.4$ mM^{-1} cm^{-1}), calculated from the absorbance at 280 nm of a sample whose concentration had been determined by amino acid analysis at the Advanced Protein Technology Centre (Hospital for Sick Children, Toronto, ON, Canada).

Steady-State Kinetics. Steady-state measurements were performed by monitoring absorbance on a Varian Cary 1E spectrophotometer equipped with a thermostatted cuvette holder (Varian Canada, Mississauga, ON, Canada) maintained at 5 ± 3 °C, or 25 ± 1 °C, controlled by Cary WinUV software version 2.00. The cuvette holder was modified to deliver streams of nitrogen gas over both sides of the cuvette, thus minimizing condensation on the cuvette surface at low temperature. For HPD inhibition experiments, HPD was generated *in situ* from TodF-catalyzed hydrolysis of freshly prepared 2-hydroxy-6-oxo-2,4-heptadienoate; the concentration of the latter was calculated from the previously determined molar absorptivity (*23*). Sufficient TodF enzyme was added to ensure the complete formation of HPD in approximately 2 min, after which time, HOPDA and $BphD_{LB400}$ were immediately added, and the BphD-catalyzed hydrolysis of HOPDA was spectrophotometrically monitored at 434 nm. The decay of HPD was not greatly accelerated by TodF: an ~10% loss of HPD occurred over the course of the 5 min measurement. BphD-catalyzed HOPDA hydrolysis was not affected by the presence of the TodF enzyme or by the presence of acetate at 100 μM. Steady-state rate equations were fit to data using the program LEONORA (*26*).

Transient Kinetic Experiments. Experiments were conducted using an SX.18MV stopped-flow reaction analyzer (Applied Photophysics, Ltd., Leatherhead, U.K.) equipped with a photodiode array detector. The temperature of the drive syringe chamber and optical cell was controlled by circulating water. For wavelengths below 350 nm, a deuterium lamp was employed to improve the signal-to-noise ratio, whereas a Xe lamp was used for wavelengths above 350 nm. The concentrations of reactants and buffer conditions were varied as described in Results. For each experiment, the data are averages of three replicates, and each replicate is generated by averaging at least five shots of the stopped-flow drive syringe. Single- or double-exponential equations were fit to the averaged time courses for single wavelength data using the SX18MV software running on the system's Acorn A5000 computer and the RISC OS 3.7 operating system. These fits provided the reciprocal relaxation times ($1/\tau$) and amplitudes; good fits are characterized by random variation in the fit residuals. Multiple wavelength data from the time courses of single turnover experiments were exported to Excel (Microsoft, Redmond, WA) and then averaged. Selected single wavelengths of the averaged data were analyzed using the SX18MV software.

HPLC Assay for the Coupling of Substrate Consumption to Product Formation. Separations were performed on a Waters 2695 system (Waters, Mississauga, ON, Canada) equipped with a Hewlett-Packard ODS Hypersil C_{18} column (5 μm, 125 × 4 mm) column, operating at a flow rate of 1

mL/min. Sample injections of 95 μL were eluted with 55% methanol and 45% water containing 0.5% phosphoric acid. Benzoic acid was quantified by comparing peak areas at 230 nm to those of standards containing known concentrations (5, 20, 100, and 250 μM) of benzoic acid. To 4 mL of potassium phosphate buffer ($I = 0.1$ M) at pH 7.5 containing 94.6 μM HOPDA (calculated using $\epsilon_{434} = 25.7$ mM^{-1} cm^{-1} (*3*)) was added sufficient $BphD_{LB400}$ to permit complete conversion in 35 min. The reaction was monitored spectrophotometrically at 434 nm, and a 200 μL aliquot was removed at each increment of 10% conversion (judged by A_{434}) and immediately quenched into 244 μL of methanol (containing 0.41% phosphoric acid). The quenched reaction solutions were analyzed by HPLC as described above (retention times: HPD, 1.6 min; benzoic acid, 2.0 min; HOPDA, 2.9 min).

Deuterium Incorporation. Deuterated buffer was prepared by evaporating 700 μL of potassium phosphate buffer ($I =$ 5 mM) at pH 7.5 and resuspending in the same volume of deuterium oxide. To 700 μL of deuterated or nondeuterated buffer was added a small volume of concentrated HOPDA dissolved in ethanol such that the final HOPDA concentration was 1 mM, and the solution contained 2% ethanol. $BphD_{LB400}$ (8 μL) was added, and the reaction was followed spectrophotometrically at 434 nm until completion (<4 min). Immediately upon reaction completion, 7 μL of 2 N HCl was added, and the reaction was extracted three times with 0.5 volumes of ethyl acetate and then evaporated under a stream of nitrogen gas. The dried sample was redissolved in acetone-d_6 and transferred to an NMR tube for analysis using a Varian 500 MHz NMR spectrometer (Varian Inc., Mississauga, ON, Canada). A reaction was also quenched approximately 1 min after completion to allow for the observation of ketonized HPD ((*E*)-2-oxo-3-pentenoic acid). Found for HPD: ^{1}H NMR (acetone-d_6, 500 MHz) δ 5.18 (1H, dd, $J_{4,5E} = 10.3$ Hz, $J_{5Z,5E} = 1.9$ Hz, H-5$_E$), 5.39 (1H, dd, $J_{4,5Z} = 17.2$ Hz, $J_{5Z,5E} = 1.9$ Hz, H-5$_Z$), 6.21 (1H, d, $J_{3,4} = 11.0$ Hz, H-3), 6.77 (1H, dt, $J_{4,5Z} = 17.0$ Hz, $J_{3,4} = 10.7$ Hz, $J_{4,5E} = 10.7$ Hz, H-4); for (*E*)-2-oxo-3-pentenoic acid: ^{1}H NMR (acetone-d_6, 500 MHz) δ 6.59 (1H, d, $J_{3,4} = 15.6$ Hz, H-3), 7.15 (1H, dq, $J_{3,4} = 15.8$ Hz, $J_{4,5} = 6.7$ Hz, H-4). The acetone signal obscured the signal from H-5 of the latter compound (expected at 2.15 ppm). Nevertheless, the H-3 and H-4 chemical shifts and coupling constants agreed with a previous report (*27*).

Mass Spectrometric Analysis of $BphD_{LB400}$ S112C. To check for Cys112 oxidation in the $BphD_{LB400}$ S112C crystals, the protein was digested with trypsin, and the proteolytic fragment containing Cys112 was analyzed by mass spectrometry. About 70 μg of protein (~2 mg/mL) in buffer (130 mM Tris-Cl at pH 8.0, and 5.8 M urea) was heated at 95 °C for 15−20 min. To the denatured enzyme (36 μL) was added 182 μL of buffer (50 mM Tris-Cl at pH 8.0, and 1 mM $CaCl_2$) to dilute the urea to <1 M. Then, 20 μg of this diluted denatured protein solution was mixed with acetonitrile (10% v/v) and trypsin (0.3 μg). Trypsin digestion occurred overnight at 37 °C, and complete digestion was confirmed by SDS−PAGE. The masses of HPLC-resolved peptides were determined using an Applied Biosystems API 300 triple quadrupole mass spectrometer with an electrospray ionization source at the Laboratory of Molecular Biophysics, University of British Columbia.

Crystallization, Preparation of Complex, and Data Collection. Crystallization experiments were performed at 20 °C using the hanging drop vapor diffusion method (*28*). Suitable crystals for diffraction experiments were obtained using reservoir solutions containing 1.8−2.4 M ammonium sulfate and 6−10% ethanol in 100 mM Tris buffer at pH 8.2. Selenomethionyl $BphD_{LB400}$, wild-type $BphD_{LB400}$, and $BphD_{LB400}$ S112C were all crystallized using similar conditions. The crystals could diffract to ~2.0 Å with Cu-Kα X-rays from a 5-kW rotating anode X-ray generator (Rigaku/MSC). To prepare crystals for flash freezing, they were loop-transferred from the growth drop into 2−5 μL of the reservoir solution augmented with 20−25% glycerol and immediately immersed in liquid nitrogen. To introduce the substrate, S112C crystals were first loop-transferred from the growth drop into 200−300 μL of the reservoir solution augmented with ~10 mM HOPDA for about 1 h. Thereafter, the crystals were loop-transferred into 200−300 μL of the reservoir solution plus 20−25% glycerol for several minutes before immersion in liquid nitrogen.

All final diffraction data were collected at cryogenic temperatures (ca. 100 K) using flash-frozen crystals and various beamlines at the Advanced Photon Source (APS), Argonne National Laboratory (Argonne, IL). For wild-type $BphD_{LB400}$, high-resolution data (1.6 Å) were collected at the BioCARS beamline 14-BMD using a Quantum-1 CCD detector (Area Detector Systems Corporation, Poway, CA). Multiwavelength anomalous diffraction (MAD) data were collected from a single crystal of selenomethione-substituted enzyme, also by the use of a Quantum-1 CCD detector at beamline 14-BMD. Both S112C and S112C + HOPDA complex data to 1.6 Å were collected at the Structural Biology Center beamline 19-ID. Programs from the HKL and HKL2000 software packages were used for diffraction data analysis (*29*). In addition, a data set was obtained at beamline 14-BMD from an S112C crystal, crystallized and frozen under anaerobic conditions. This experiment was a successful attempt to prevent the oxidation of active site cysteine, which was consistently observed for S112C crystals grown in air and exposed to X-rays. For this experiment, the cryopreservative solution was augmented with 10 mM ascorbate, which was added to provide a free radical scavenger (*30*). A short exposure time was used to reduce total X-ray exposure. HKL2000 was used for data processing (*29*).

Structure Determination and Refinement. The structure of selenomethionine-modified $BphD_{LB400}$ was determined using the multiple wavelength anomalous diffraction (MAD) method. $BphD_{LB400}$ crystals have space group $P6_4$ with two monomers per asymmetric unit. The program SOLVE (*31*) was used to locate 19 crystallographically unique Se atoms by an analysis of data from the three-wavelength MAD experiment. The Se positions were refined with MLphare from the CCP4 suite (*32*). The initial phases were improved through solvent-flattening and histogram-matching by use of the program DM, also from the CCP4 suite. The secondary structure was easily recognized in the electron density maps, and the initial model with side chains was constructed with the O program (*33*), which was used for all subsequent electron density interpretation and model fitting. All atomic models were refined using the CNS program (*34*). After one round of refinement at 2.0 Å resolution, the phases were extended to 1.6 Å.

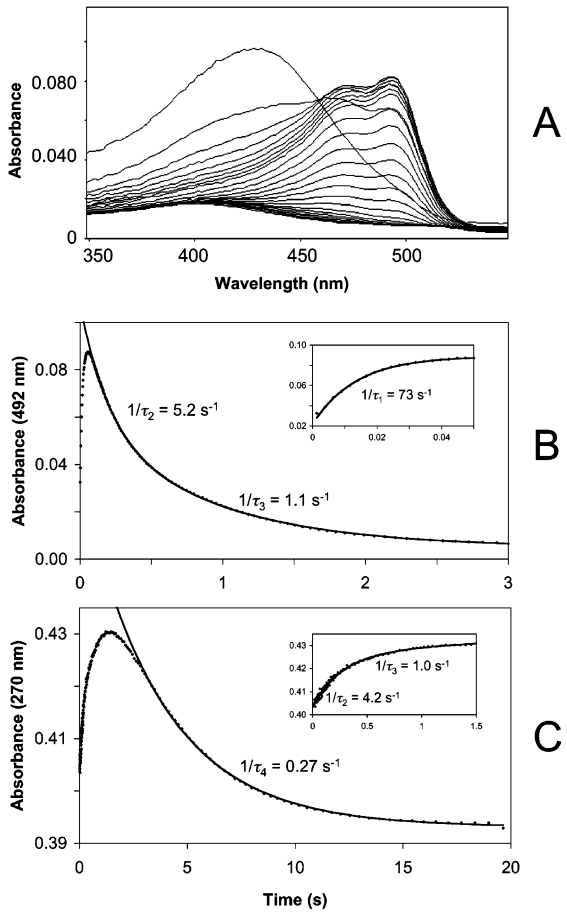

FIGURE 3: Representative stopped-flow experiment illustrating a single turnover of HOPDA (4 μM) by $BphD_{LB400}$ (8 μM) at 3.2 °C in potassium phosphate buffer supplemented with 20% glycerol (I = 100 mM) at pH 7.5. (A) Time-resolved spectral changes show free HOPDA (λ_{max} = 434 nm) transformed into an enzyme-bound form, E:S (λ_{max} = 492 nm). (B) Absorbance at 492 nm vs time shows the decay of the E:S intermediate. The solid line denotes the double exponential fit. The inset shows the single-exponential fit for the formation of the E:S intermediate. (C) Absorbance at 270 nm vs time for the formation/decay of the HPD product. Data points are shown together with the fit of a single exponential (solid line) describing HPD decay. The inset shows the formation of HPD and its fit to a double exponential.

RESULTS

Single Turnover Stopped-Flow Kinetic Analysis. $BphD_{LB400}$ catalyzed the hydrolysis of HOPDA to benzoate and HPD with a k_{cat} of 6.5 ± 0.5 s^{-1} at 25 °C. This value is slightly higher than that previously reported (*3*, *23*, *35*), which may result from a more accurate determination of protein concentration (see Materials and Methods). We performed stopped-flow experiments using a diode array detector to resolve and spectrophotometrically characterize intermediates during a single catalytic cycle. Figure 3 illustrates data from an experiment performed under slow conditions (T = 3.2 °C, 20% glycerol). Using a 2:1 ratio of enzyme (8 μM) to substrate (4 μM), the HOPDA enolate (λ_{max} = 434 nm) was rapidly transformed into a species with absorbance maxima at 473 and 492 nm (Figure 3A). Indeed, at 25 °C, the transformation was approximately 50% complete within the dead time of the instrument (~1.2 ms), indicating a process occurring with reciprocal relaxation time, $1/\tau_1 \approx 500$ s^{-1} (*36*).[2] The red-shifted spectrum of the E:S species may arise from a deprotonated form of HOPDA (enolate) or a ketonized HOPDA, as discussed below. The E:S intermediate decayed in a biphasic manner (at 25 °C, $1/\tau_2 = 54 \pm 4$ s^{-1}, $1/\tau_3 = 5.8 \pm 0.9$ s^{-1}), with similar phase amplitudes (Figure 3B, Table 1). Concurrent with E:S decay was a biphasic increase at 270 nm, the absorbance maximum of HPD (at 25 °C, $1/\tau_2 = 48 \pm 12$ s^{-1}, $1/\tau_3 = 8.3 \pm 0.7$ s^{-1}), followed by a slower monotonic decay (Figure 3C). The decay of HPD is due to ketonization to the more stable α/β-unsaturated ketone, a process that occurs nonenzymatically on a time scale of minutes (*37*). The faster rate observed in this experiment is due to enzyme-catalyzed ketonization, as observed with MhpC (*37*). In contrast to the relatively equal distribution of phase amplitudes for $1/\tau_2$ and $1/\tau_3$ at 492 nm, the amplitude of $1/\tau_3$ at 270 nm was only ~10% of the total absorbance change (Table 1). We attribute this to the enzyme-catalyzed decay of HPD, which reduces the amplitude associated with phase 3, and, thereby, makes $1/\tau_2$ and $1/\tau_3$ difficult to resolve at 270 nm. Performing the experiment at 3.2 °C better resolved the two phases at 270 nm. Under these conditions, $BphD_{LB400}$ catalyzed HOPDA hydrolysis with a $k_{cat} = 0.98 \pm 0.06$ s^{-1} and $K_m = 0.30 \pm 0.08$ μM. Indeed, this experiment generated values of $1/\tau_2$ (~10 s^{-1}) and $1/\tau_3$ (~1.5 s^{-1}) with corresponding amplitudes at 270 nm that matched those at 492 nm (Table 1).

Kinetic experiments were performed in the presence of 20% glycerol to help assign relaxations to bimolecular events. Specifically, increasing solvent viscosity should slow diffusive events that reflect association/dissociation from the enzyme. The presence of glycerol did not affect the steady-state kinetic parameters. In contrast, glycerol slowed two of

Table 1: Reciprocal Relaxation Times and Amplitudes for Single-Turnover Reactions[a]

T (° C)	glycerol (% v/v)	wavelength (nm)	phase 1[b]	phase 2[c] (% total amplitude)	phase 3[c] (% total amplitude)	phase 4[d]
25	0	270 (HPD)		48 ± 12 s^{-1} (89)	8.3 ± 0.7 s^{-1} (11)	0.59 ± 0.04 s^{-1}
		492 ($E:S^k$)	~500 s^{-1}	54 ± 4 s^{-1} (68)	5.8 ± 0.9 s^{-1} (32)	
	20	270 (HPD)		34 ± 2 s^{-1} (51)	5.3 ± 0.3 s^{-1} (49)	0.71 ± 0.01 s^{-1}
		492 ($E:S^k$)	~200 s^{-1}	33 ± 2 s^{-1} (66)	5.5 ± 0.4 s^{-1} (34)	
3.2	0	270 (HPD)		12 ± 2 s^{-1} (51)	2.3 ± 0.6 s^{-1} (49)	0.22 ± 0.01 s^{-1}
		492 ($E:S^k$)	~200 s^{-1}	8.7 ± 0.3 s^{-1} (49)	1.3 ± 0.2 s^{-1} (51)	
	20	270 (HPD)		3.8 ± 0.4 s^{-1} (68)	1.0 ± 0.1 s^{-1} (32)	0.25 ± 0.03 s^{-1}
		492 ($E:S^k$)	66 ± 6 s^{-1}	4.5 ± 0.8 s^{-1} (49)	1.2 ± 0.1 s^{-1} (51)	
	20[e]	270 (HPD)		4.0		0.41 s^{-1}
		492 ($E:S^k$)	~130	4.4 s^{-1} (45)	1.1 s^{-1} (55)	

[a] The errors are reported as the standard deviation of three measurements. [b] Phase 1 represents the rapid formation of E:S. [c] The amplitudes are reported as a percentage of the total amplitude of phase 2 and phase 3 combined. [d] Represents the enzyme-catalyzed ketonization of HPD. [e] A single measurement performed with a 6:1 ratio of enzyme (20 μM) to substrate (4 μM).

Scheme 1

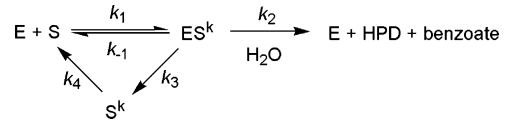

the observed relaxations at 3.2 °C: $1/\tau_1$, the rate of formation of E:S, was reduced from ~200 s^{-1} to 66 ± 6 s^{-1}, and $1/\tau_2$ was reduced by ~50% at both 270 and 492 nm (Table 1). Even at the slowed rate, the formation of E:S occurred with an apparent isosbestic point at 460 nm, implying a single-step transformation from HOPDA (Figure 3A). The reduction in $1/\tau_2$ is consistent with this step, representing HPD dissociation. The inverse relationship of solvent viscosity and rate of diffusive product release from an enzyme is well documented. For example, viscosity effects on k_{cat} have been used to demonstrate the rate-determining dissociation of the ADP product from protein kinases (*38*, *39*). Finally, $1/\tau_3$ was not affected by glycerol, suggesting that this step involves an intramolecular event rather than diffusive product release.

In the event that the high-wavelength spectrum represents enzyme-bound ketonized HOPDA ($E:S^k$), it is possible that the glycerol-induced decrease of $1/\tau_2$ reflected dissociation of ketonized HOPDA (S^k) from the enzyme, as proposed for MhpC (Scheme 1) (*12*). In such a scenario, S^k dissociation and hydrolysis would have similar rate constants ($k_2 \approx k_3 \approx$ 25 s^{-1} at 25 °C) such that 50% of the substrate is initially turned over to product, while 50% is released as S^k. Thus, re-enolization of the released S^k ($k_4 \approx 6$ s^{-1}) would limit the rate of hydrolysis of 50% of the substrate such that $1/\tau_3 \approx 6$ s^{-1} would comprise 50% of the amplitude of $E:S^k$ decay. However, $1/\tau_2$ exhibits the same behavior at both 492 nm ($E:S^k$ decay) and 270 nm (HPD formation), suggesting that $E:S^k$ processing is directly coupled to HPD formation. Hence, a kinetic model involving the release of S^k does not satisfactorily account for the biphasic relaxation. The release of S^k was further ruled out as described below.

To investigate whether the biphasic kinetics reflected multiple turnovers, an experiment was conducted at 3.2 °C with 20% glycerol using a 5:1 ratio of enzyme (20 μM) to substrate (4 μM). In this experiment, the values and amplitudes of $1/\tau_2$ and $1/\tau_3$ were essentially identical to those observed using a 2:1 ratio (Table 1), indicating that the relaxations do not reflect multiple turnovers.

We also investigated whether the biphasic kinetics resulted from (a) a product complex absorbing at 492 nm but with a molar absorptivity of ~50% of E:S or (b) the use of phosphate buffer. In a stopped-flow experiment performed by mixing the enzyme (8 μM) with excess HPD (~500 μM) and benzoate (1.0 mM), no absorbance at 492 nm was detected (data not shown). Moreover, in a single turnover experiment ($E = 8$ μM; $S = 4$ μM) performed using a Na-HEPES buffer ($I = 100$ mM at pH 7.5), the amplitudes and rates of the observed relaxations were essentially identical to those observed using the phosphate buffer. Thus, neither the phosphate nor the absorbance of a product complex influenced the kinetic behavior of BphD.

Coupling of Substrate Consumption to Product Formation. A branched pathway (Scheme 1) involving the partial release of the keto-intermediate (S^k) has been proposed for MhpC on the basis of deuterium exchange and stopped-flow studies (*11*, *12*). Subsequent crystallographic observation of apparent half-site reactivity suggested that release occurs from an inactive subunit (*20*). Such release followed by rate-limiting re-enolization of S^k in solution may account for the biphasic kinetics observed in the single-turnover stopped-flow experiments, even though it was not supported by the apparent coupling of $E:S^k$ decay (492 nm) and HPD formation (270 nm) (see above). Significantly, this model predicts a considerable steady-state population of S^k. In an attempt to detect S^k accumulation during the turnover of $BphD_{LB400}$, we simultaneously monitored HOPDA consumption and benzoate production in a reaction performed at 25 °C ($I = 100$ mM potassium phosphate buffer at pH 7.5). More specifically, HOPDA consumption was monitored by absorbance at 434 nm. As the reaction proceeded, aliquots were removed at intervals corresponding to increments of 10% completion and quenched in acidic solution, and benzoate was quantified by HPLC analysis. At all intervals, the amount of benzoate detected corresponded to the amount of HOPDA consumed within the margin of error (±5%; data not shown). These results indicate that significant amounts of S^k did not accumulate in solution during turnover. Failure to detect significant quantities of S^k in solution during turnover suggests two possibilities: (1) S^k is not released from the enzyme, or (2) the re-enolization of S^k in solution is faster than release, in which case, it could not be responsible for the biphasic kinetics.

Deuterium Incorporation into HPD. To further investigate the possibility of S^k release during catalytic turnover and to confirm the stereochemical course of the reaction with native enzyme, we analyzed the incorporation of deuterium from D_2O into HPD during the $BphD_{LB400}$-catalyzed hydrolysis of HOPDA. Studies using His_6-tagged $BphD_{LB400}$ (*40*) have demonstrated that the enzyme stereospecifically incorporates deuterium into the H-5_E position of HPD. To minimize nonspecific exchange at H-5_Z of HOPDA that might occur via phosphate-catalyzed ketonization similar to that reported for 2-hydroxymuconate (*41*), we lowered the phosphate buffer concentration to $I = 5$ mM. Under these conditions, deuterium exchange at H-5 of HOPDA occurred with a half-life of ~10 min, which was about twice as fast as the exchange into H-3. These rates were approximately one-third as fast as that at $I = 100$ mM phosphate. Moreover, sufficient amounts of $BphD_{LB400}$ were added to ensure that HOPDA hydrolysis was complete in less than 4 min.

Figure 4 shows the ^1H NMR spectrum of HPD from a reaction performed in D_2O. Peak integration revealed that ~10% signal loss occurred at H-5_Z during the course of an enzyme-catalyzed reaction. This small amount of deuterium incorporation corresponded to what was observed over a similar time period in the absence of $BphD_{LB400}$. By contrast, almost complete deuterium incorporation occurred at H-5_E, as predicted.[3] Hence the enzyme stereospecifically incorporates a proton at H-5_E, and the nonspecific incorporation at

[2] For an instrument dead time of 1.2 ms, only ~50% of a reaction with $1/\tau = 500$ s^{-1} may be observed. The observable fraction of the reaction (f_{obs}) can be determined from the instrument dead time (t_d) and the half-life of the reaction ($t_{1/2}$) as follows: $f_{obs} = (1/2)^{\wedge}(t_d/t_{1/2})$ (*36*).

[3] The reaction contained 1% water (from the addition of aqueous BphD) and 2% ethanol (from the addition of concentrated HOPDA), thereby causing a small signal from H-5_E.

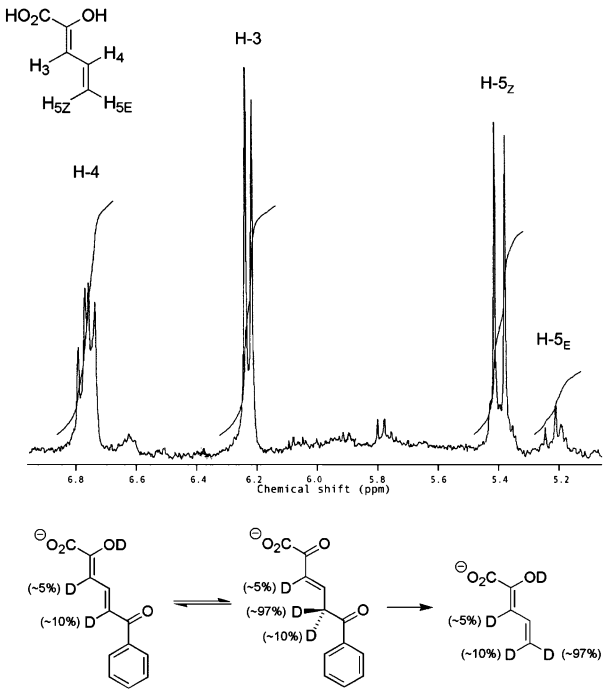

FIGURE 4: Top: The ^{1}H NMR spectrum of HPD generated from $BphD_{LB400}$-catalyzed hydrolysis of HOPDA in 97% D_2O (potassium phosphate, pD 7.5, $I = 5$ mM). Peak integration demonstrates ~10% deuterium incorporation into H-5_Z and almost complete incorporation into H-5_E. Bottom: The ~10% nonspecific deuterium incorporation into H-5_Z is consistent with nonenzymatic exchange prior to enzymatic catalysis.

H-5_Z can be explained by nonenzymatic exchange prior to enzymatic hydrolysis. If the reaction was allowed to continue after the complete conversion of HOPDA, ketonized HPD ((*E*)-2-oxo-3-pentenoate) appeared in the NMR spectrum (data not shown). Indeed, the addition of $BphD_{LB400}$ to a solution of HPD confirmed that the enzyme catalyzes the ketonization of HPD, as reported for MhpC (*37*).

In summary, three independent experiments indicate that S^k is not released from the enzyme in significant amounts: (1) single-turnover stopped-flow experiments showed matching biphasic behavior for both HPD formation and E:S^k decay; (2) the amount of benzoate produced in steady-state assays corresponded to the amount of HOPDA hydrolyzed; and (3) deuterium was not incorporated into HPD at H-5_Z above background levels. These results suggest that the $BphD_{LB400}$-catalyzed hydrolysis of HOPDA proceeds via a linear model as opposed to the branched model involving S^k release proposed for MhpC (*12*).

Product Inhibition. To facilitate the interpretation of transient state kinetic data, product inhibition studies were performed (potassium phosphate buffer ($I = 100$ mM) at pH 7.5) under two conditions representative of those used for the single-turnover experiments: (1) 25 ± 1 °C and (2) 5 ± 3 °C, 20% glycerol. In these experiments, inhibition by each product (benzoate and HPD) was examined by steady-state kinetics so as to probe the order of product release. At 25 °C, benzoate was found to competitively inhibit $BphD_{LB400}$-catalyzed hydrolysis of HOPDA with $K_{ic} = 165 \pm 20$ μM (data not shown). Under these conditions, however, HPD was not sufficiently stable to reliably characterize inhibition. At 5 °C in the presence of 20% glycerol, benzoate also competitively inhibited the $BphD_{LB400}$-catalyzed hydrolysis of HOPDA with $K_{ic} = 220 \pm 30$ μM (Figure 5A). This result indicates that benzoate competes for the active site of the free enzyme and, therefore, may be the last product released from the enzyme. Under these same conditions, HPD inhibited the $BphD_{LB400}$-catalyzed hydrolysis of HOPDA in a mixed fashion with $K_{ic} = 84 \pm 41$ μM and $K_{iu} = 120 \pm 30$ μM (Figure 5B). This indicates that HPD is released in a step that generates an enzyme species other than that which binds the free substrate (*42*). The competitive component of the mixed inhibition suggests that HPD may also bind to the free enzyme (E:HPD). Consistent with this hypothesis, $BphD_{LB400}$ catalyzed the ketonization of HPD (see single turnover stopped-flow results). The results should be regarded with some caution because there will inevitably be some ketonized HPD present in the reaction even at low temperature. However, the product inhibition experiments are consistent with a mechanism in which HPD is released prior to benzoate, but the former may reassociate with the free enzyme to undergo ketonization.

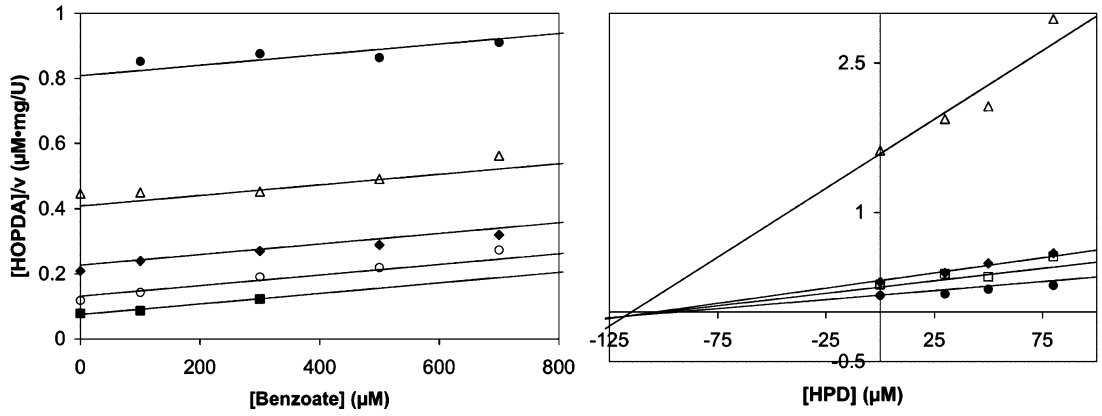

FIGURE 5: Cornish-Bowden plots illustrating the type of inhibition of the $BphD_{LB400}$-catalyzed hydrolysis of HOPDA by reaction products. (A) Inhibition by benzoate described by competitive inhibition ($K_{ic} = 220 \pm 30$ μM; $K_m = 0.21 \pm 0.02$ μM; $V = 5.9 \pm 0.2$ U/mg). The reaction rates determined using 0.24 (■), 0.57 (○), 1.1 (◆), 2.2 (△), and 4.6 μM (●) HOPDA. (B) Inhibition by HPD described by mixed inhibition ($K_{ic} = 84 \pm 41$ μM; $K_{iu} = 120 \pm 30$ μM; $K_m = 0.45 \pm 0.08$ μM; $V = 4.0 \pm 0.2$ U/mg). The reaction rates were measured using 0.23 (●), 0.56 (□), 0.82 (◆), and 5.9 μM (△) HOPDA. Equations describing competitive, uncompetitive, and mixed inhibition were each fit to the data using the least-squares, dynamic weighting options of the LEONORA program, and the type of inhibition determined by comparing the quality of fit based on nonrandom trends in the residuals. The solid lines represent the best fit parameters of the global fit at each HOPDA concentration. Conditions: potassium phosphate buffer ($I = 100$ mM) and 20% glycerol at pH 7.5, 5 ± 3 °C.

Table 2: X-ray Diffraction Data

crystal type	wild-type	SeMet BPHD−MAD phasing			S112C	S112C + HOPDA	$S112C_{anaerobic}$
		inflection	peak	remote			
wavelength (Å)	0.9795	0.9795	0.9793	0.9537	0.9783	0.9783	0.9000
resolution (Å)	50−1.6	50.0−2.0	50.0−2.0	50.0−2.0	50−1.6	50−1.6	50−1.9
space group	$P6_4$	$P6_4$	$P6_4$	$P6_4$	$P6_4$	$P6_4$	$P6_4$
a (Å)	135.00	136.50	136.50	136.48	135.08	135.51	135.06
c (Å)	66.73	66.03	66.03	66.03	66.28	66.62	66.30
observations	750379	1610683	1637855	1684790	2008833	1663889	1387384
unique reflections	88102	47880	48007	47694	90566	91070	52538
R_{sym} (%)[a] (last shell)	6.0 (35.9)	4.9 (30.9)	5.1 (34.1)	4.4 (28.6)	8.9 (41.8)	4.5 (39.7)	8.2 (62.5)
average $I/\sigma(I)$ (last shell)	22.6 (2.7)	27.6 (2.9)	26.2 (2.7)	29.9 (3.4)	20.1 (2.1)	38.8 (3.4)	14.2 (1.8)
completeness (%) (last shell)	96.6 (73.9)	92.1 (59.2)	92.5 (59.3)	95.4 (72.9)	99.8 (98.9)	99.7 (99.4)	96.3 (90.9)

[a] $R_{sym} = \sum_{hkl}\sum_{i=1}^{n} | I_{hkl,i} - \bar{I}_{hkl}| / \sum_{hkl}\sum_{i=1}^{n} I_{hkl,i}$

Table 3: Refinement Statistics and Characteristics of the Refined Atomic Models

crystal type	wild-type	S112C	S112C + HOPDA	$S112C_{anaerobic}$
		model content		
protein residues	568	568	568	568
substrate (HOPDA)	0	0	1	0
glycerol molecules	1	3	3	1
ethanol molecules	3	9	6	1
sulfate molecules	4	2	1	3
water molecules	469	404	338	336
		refinement statistics		
resolution range (Å)	50−1.6	50−1.6	50−1.6	50−1.97
R, R_{free} (%)	20.8, 22.5	20.3, 21.4	20.8, 22.5	19.7, 22.5
last shell R, R_{free} (%)	28.8, 34.7	26.4, 29.4	27.9, 29.1	25.9, 25.5
		average *B*-factors (Å^2)		
protein atoms[a]	A 16.0	A 17.4	A 21.2	A 26.1
	B 37.1	B 34.8	B 42.9	B 46.2
water atoms	32.2	32.4	35.3	40.4
all atoms	27.1	26.5	32.3	36.5
		RMSD[b] from restraints		
bond lengths (Å)	0.0048	0.0049	0.0048	0.0054
bond angles (°)	1.16	1.17	1.16	1.15

[a] The labels A and B identify atoms from crystallographically independent monomers. [b] Root-mean-square deviation.

Kinetic Behavior of the Ser112Cys Mutant. To help obtain a crystal structure approximating the E:S complex, the active site Ser112 of $BphD_{LB400}$ was substituted with cysteine. This substitution was expected to lower the rate of HOPDA hydrolysis, perhaps to the point where the complex could be formed in the crystal and trapped by rapid freezing. Attempts to measure steady-state kinetic parameters for the S112C variant were confounded by the nonlinearity of the progress curves, indicative of strong product inhibition or enzyme inactivation. The inclusion of 1 mM DTT did not affect the nonlinearity, suggesting that the latter was not due to the oxidation of Cys112. Nevertheless, estimates of initial velocities at 25 °C generate $k_{cat} = 0.27 \pm 0.02$ s^{-1} and $K_m = 2.8 \pm 0.6$ μM and a specificity constant ($k_{cat}/K_m = 9.5 \pm 2.2 \times 10^4$ M^{-1} s^{-1}) approximately 240-fold lower than that of the wild-type enzyme. In a single turnover stopped-flow experiment at 25 °C, the high wavelength intermediate observed in the wild type failed to accumulate. However, the HOPDA signal at 434 nm decayed in a biphasic manner ($1/\tau_1 = 2.6$ s^{-1}, amplitude = 0.063; $1/\tau_2 = 0.25$ s^{-1}, amplitude = 0.019, where $1/\tau_1$ and $1/\tau_2$ apparently correspond to $1/\tau_2$ and $1/\tau_3$, respectively, in the wild type). As in the wild type, HPD (at 270 nm) also displayed biphasic formation ($1/\tau_1 = 4.7$ s^{-1}, amplitude = 0.012; $1/\tau_2 = 1.0$, amplitude = 0.014). The S112C substitution apparently slowed the initial reaction because the red-shifted spectrum of E:S did not accumulate. Nevertheless, the biphasic disappearance of the HOPDA signal seems approximately coupled to the formation of HPD, a pattern not unlike that observed in the wild type.

Crystal Structures. Table 2 summarizes the crystallographic data used for initial phase determination and model refinement. The final phasing powers were 4.59 and 2.47 for acentric and centric reflections measured at the wavelength corresponding to the peak of the absorption spectrum and 4.26 (acentric) and 2.20 (centric) for data measured at the wavelength of the inflection point of the absorption edge. The mean figure of merit was 0.75 for all data after MAD phasing and 0.85 after density modification.

The refined models of the wild type, S112C, S112C (anaerobic), and S112C + HOPDA are of high reliability as demonstrated by the data in Table 3. The two crystallographically independent molecules of $BphD_{LB400}$ are labeled A and B. The atomic model of A does not include the *N*-terminal residue and that of B does not include the three *N*-terminal residues.

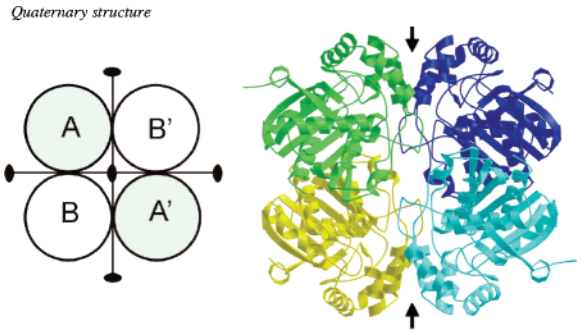

FIGURE 6: Left: Schematic diagram of $BphD_{LB400}$ shown as a tetramer with 222-point group symmetry. The view is down a crystallographic 2-fold axis parallel to the *c* axis of the crystal. A and B are crystallographically independent: crystallographic 2-fold symmetry transforms A into A′ and B into B′. In contrast, A is related to B or B′ by noncrystallographic 2-fold symmetry. Right: Ribbon diagram of the $BphD_{LB400}$ tetramer viewed in the same direction. The four subunits are colored green, yellow, cyan, and blue. Arrows highlight the close contacts between the lid domains of A and B′ (and A′ and B).

Quaternary Structure. As observed in solution (*24*), $BphD_{LB400}$ is a tetrameric oligomer in the crystal (Figure 6). The tetramer is formed by the back-to-back interaction of two A−B dimers related by crystallographic 2-fold symmetry. Two noncrystallographic 2-fold axes relate A to B or B′. These axes are perpendicular to each other and to the crystallographic 2-fold axis, thereby generating a tetramer with approximate 222 (D_2) point group symmetry. Of the three interfaces in the tetramer, the AB interface has the largest buried surface area, 2039 Å^2 as calculated using GRASP (*43*). Considerably smaller surface areas of 1135 and 964 Å^2 were calculated for the AB′ interface and the AA′ interface, respectively. The A−B dimer interaction involves the β8 strands from both subunits forming an antiparallel β pair and corresponds to the 1−5 interaction of the $BphD_{RHA1}$ octamer (*17*). Similar interactions were also found in $CumD_{IP01}$ (*18*), $CarC_{J3}$ (*19*), and MhpC (*20*), suggesting that the A−B dimer is a basic structural unit from which some members of this family, such as $BphD_{LB400}$ and $BphD_{RHA1}$, may construct higher oligomers.

The crystallographically independent monomers (A and B) have highly similar structures (RMSD of 0.53 Å for the superposed Cα atoms). Subunit A has better electron density and lower *B* factors (Table 3). In addition, α9 of the lid domain is closer to the core domain in subunit A. These differences can be explained by crystal packing: the A subunits pack against each other and are further surrounded by B subunits, whereas each B subunit is open to one of the large solvent channels located about the crystal's 6_4 screw axes.

Monomer Structure. $BphD_{LB400}$ comprises two domains: a core domain (residues 2−145 and 213−286) containing the canonical α/βhydrolase fold (*7*−*9*) and a lid domain (residues 146−212) (Figure 7). The core domain primarily consists of a highly twisted eight-stranded β sheet with five helices on each side of the sheet. The lid domain consists of five helices, including one 3_{10} helix, and occurs as an insertion in the core domain's canonical fold.

The fold of $BphD_{LB400}$ is similar to those of other MCP hydrolases. An overlay of Cα atoms of $BphD_{LB400}$, $BphD_{RHA1}$, MhpC, $CarC_{J3}$, and $CumD_{IP01}$ showed that the β sheet

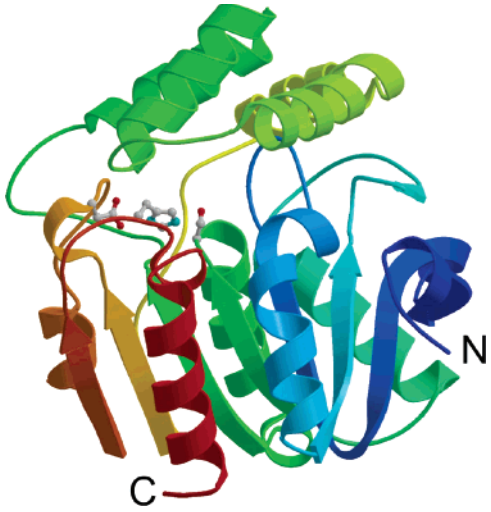

FIGURE 7: Ribbon diagram of $BphD_{LB400}$ subunit A. The lid domain (residues 146−212) is shown at the top, and the key catalytic residues (Asp237, His265 and Ser112) are shown in ball-and-stick representation.

and some α helices superpose well; as expected, some loop regions do not. The RMSDs for Cα atoms between $BphD_{LB400}$ and MhpC (PDB entry 1U2E), $CumD_{IP01}$ (PDB entry 1IUP), $BphD_{RHA1}$ (PDB entry 1C4X), and $CarC_{J3}$ (PDB entry 1J1I) are 1.01, 1.44, 1.54, and 1.48 Å, respectively. The core domains superpose with high fidelity such that only a few short segments are not superposable. These include the *N*-terminal eight residues and loop regions between β1 and β2 (residues 16−22), between β2 and β3 (residues 32−34), and between β4 and α2 (residues 79−86; α and β numbered according to ref 17 (*17*)). Greater structural divergence is observed among the lid domains, which is consistent with low sequence identity in this region. The observed conformational variability of the lid domain may also partially result from the differential crystal packing among the five structures.

As expected, the overall subunit structures of S112C in both aerobic and anaerobic conditions and S112C + HOPDA are almost identical to those of the wild-type structure, with the RMSD of Cα atoms between them being less than 0.24 Å.

Active Site. The active site is located at the cleft between the lid and core domains and includes conserved Ser112, His265, and Asp237, reminiscent of the catalytic triad of serine proteases. The active site can be divided into two subsites, P (polar) and NP (nonpolar), located on each side of the catalytic serine. The P and NP subsites bind the dienoate moiety and phenyl ring of the substrate, respectively, and correspond to the proximal and distal parts identified in a study of $BphD_{RHA1}$ (*17*). The P subsite is lined with polar groups from the side chains of residues that are conserved in MCP hydrolases (Asn51, Asn111, Arg190, and Trp266). The NP subsite is lined with nonpolar side chains Ile153, Leu156, Phe175, Leu213, Trp216, and Phe239.

The hydrogen bonding among the catalytic residues Asp237, His265, and Ser112 is of significant mechanistic interest. In the wild-type $BphD_{LB400}$ structure, the Oδ2 atom of Asp237 forms a hydrogen bond with the Nδ1 atom of His265. The Nϵ2 atom of His265 forms a hydrogen bond with Oδ1 of Asn111 instead of the Oγ atom of Ser112 in subunit A and does not form any hydrogen bond in subunit

B. Consistent with these data, the catalytic His and Ser are not hydrogen bonded in the $BphD_{RHA1}$ and $CarC_{J3}$ structures (*17*, *19*). The His and Ser are hydrogen bonded in the MhpC structure, but the bond is longer (3.3 Å) than that typically observed in serine hydrolases (*20*). Although the observed states of these molecules may differ significantly from the catalytic states, the lack of a prominent His−Ser interaction is consistent with an alternative use of the catalytic triad.

In the structure of wild-type $BphD_{LB400}$, a water molecule is hydrogen bonded to OγSer112, a phenomenon that was also observed in the structure of native MhpC (*20*). In contrast, unexplained electron density was observed adjacent to the Oγ atom of the active site serine in $BphD_{RHA1}$ (*17*) and certain structures of MhpC (*20*), suggesting covalent modification. In the structure of the S112C variant of $BphD_{LB400}$ crystallized aerobically, electron density suggests that Cys112 is oxidized to the sulfonic acid in subunit A and to the sulfenic acid in subunit B (data not shown). The oxidation apparently occurred during X-ray exposure because mass spectrometric analysis of crystallized S112C before X-ray exposure indicated that Cys112 was not oxidized. Active site thiol oxidation by X-rays has been previously noted for cysteinyl hydrolases (*44*), including dienelactone hydrolase (*45*) and papain (*46*). Because dioxygen may be involved in cysteine oxidation, we anaerobically crystallized S112C and collected diffraction data from the liquid nitrogen frozen crystals maintained at 100 K under a gaseous nitrogen stream. It is clear that Cys112 is not oxidized in the anaerobic S112C structure, suggesting that oxidation requires both X-rays and dioxygen. Interestingly, in the active site of the anaerobic S112C structure, a water molecule is hydrogen bonded to the Sγ atom of Cys112 as that in the wild-type structure.

Enzyme−Substrate Interactions. In the crystal structure of S112C exposed to HOPDA, clear electron density is observed for the dienoate moiety of HOPDA in the active site of subunit A, whereas the electron density for the phenyl moiety is partial and fragmented. The dienoate moiety is well defined as a keto tautomer because C6 clearly lies out of the C1−C2−C3−C4−C5 plane, implying saturation at C5. Similar electron density was observed in subunit B but was less clearly defined. Although the density permitted the modeling of a complete substrate molecule into the active site of subunit A and subsequent refinement, it only marginally supports the inclusion of the phenyl moiety in the model. More significantly, the density is continuous between C112 Sγ and C6 of the ligand and includes a feature that could represent the C6 hydroxyl substituent bound in the vicinity of the oxyanion hole. The density affords two possible interpretations. In one, the structure would be described as a covalent, tetrahedral intermediate with C6 of the substrate bonded to Cys112 (Figure 8). However, the discrete existence of such a transient catalytic intermediate on the time scale of the HOPDA soak-in (∼1 h) is unlikely. A more probable interpretation is suggested by the absence of clear density for the phenyl ring and the X-ray-induced oxidation of Cys112 observed in the absence of the substrate. In this case, the density is explained by the combination of density for the product (HPD) in some but not all active sites and density for oxidized C112, perhaps in different conformations with and without the product present. Hence, we refer to this structure as S112C + HOPDA to indicate how the crystal was prepared and to emphasize that the existence of a catalytically relevant tetrahedral intermediate at C6 in this structure is unlikely. In any case, the most important feature of this structure is the clear density for the dienoate moiety, which suggests important enzyme−substrate interactions in this region of the active site.

The S112C + HOPDA structure reveals a series of hydrogen bonds between conserved residues in the P subsite (Gly43, Asn51, Arg190, His265, Trp266, and Asn111) and the dienoate moiety of the substrate (Figure 8, Table 4). The Nη1 and Nη2 atoms of Arg190, the N atom of Gly43, the Nδ2 atom of Asn51, and the Nϵ1 atom of Trp266 interact with the C1 carboxylate of the substrate, whereas the Nδ2 atom of Asn111, the Nϵ2 atom of His265, and the Nϵ1 atom of Trp266 interact with the C2 hydroxyl of the substrate. Significantly, a sulfate ion occupies the same position as the carboxylate and C2 hydroxyl of the substrate in both the wild-type and S112C mutant structures, indicating the important role of this enzyme pocket in stabilizing negative charge and, thereby, positioning the substrate in the correct orientation.

The crystal structure also shows that the main chain amides from residues Met113 and Gly42 are appropriately positioned to form the oxyanion hole that is typical for mechanistically related hydrolases and, thus, would stabilize an oxyanion at C6. Met113 is located at the N terminus of helix α3, suggesting that the partial positive charge at this end of α3 also may help stabilize the negative charge of the substrate oxyanion. Gly42 is located in the loop between β3 and α2. In this loop, the highly conserved His40 side chain is hydrogen bonded to the Gly41 carbonyl, thereby directing the Gly42 amide toward the substrate oxyanion.

Although the density for the substrate's phenyl ring is poor, the model places this part of the substrate so that it is entirely surrounded by hydrophobic residues (Val240, Trp216, Leu213, Ile153, Phe157, Leu156, and Phe239) in the NP subsite of the active site (Figure 8). Comparison of the wild-type and S112C structures with the S112C + HOPDA structure suggests that residues Phe175, Phe239, His265, Trp266, and Leu213 may undergo conformational changes upon substrate binding.

An examination of each of the $BphD_{LB400}$ structures indicates that the conformation of the active site is adaptable. For example, electron density maps for each of the three structures clearly indicate that important active site residues occur in multiple conformations within subunit A or within subunit B of single crystals: Trp266 in subunit A, and Met135 and Trp266 in subunit B of wild-type $BphD_{LB400}$; Met135, Phe175, Phe239, and His265 in subunit A of $BphD_{LB400}$ S112C; and Met135, Phe175, Val240, and Trp266 in subunit B of the $BphD_{LB400}$ S112C + HOPDA complex. Comparisons of active sites between subunits in the same crystal or between the same subunit in different crystals also reveal differences in conformation for several residues (Asn111, Phe175, Leu213, Phe239, Val240, His265, and Trp266). Thus, differences occur between A and B of wild-type $BphD_{LB400}$, between subunits A of the wild-type and the S112C mutant, or between subunits A of the wild-type and S112C + HOPDA. Taken together, this variability suggests that conformational changes involving these residues may be important for substrate binding or catalysis. It is interesting to note that His252 and Trp253 in

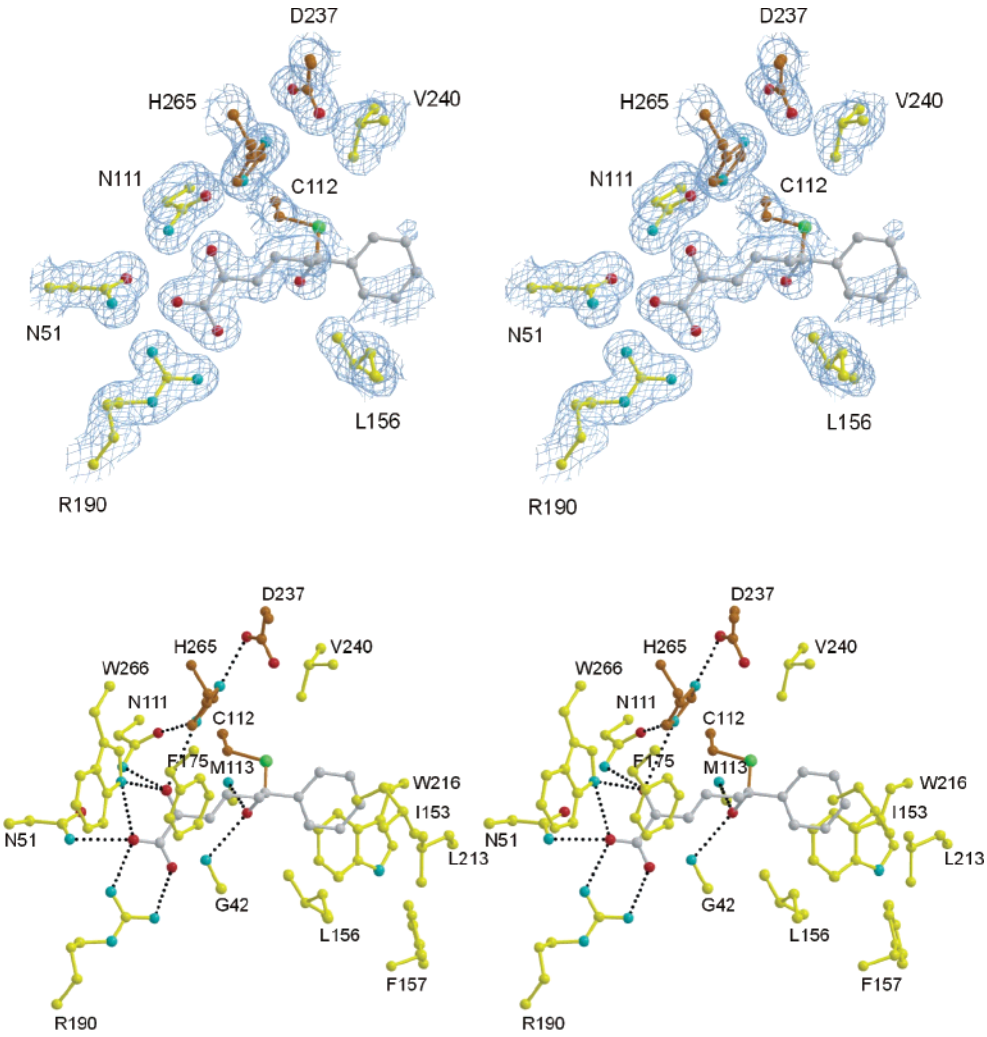

FIGURE 8: Stereoview of HOPDA bound to the active site of $BphD_{LB400}$ S112C mutant. Top: The refined structure is shown along with $(2F_o - F_c)$ exp(iα_c) electron density (1.0 σ). Bottom: Ball-and-stick stereo model of enzyme−substrate interactions. O, N, and S atoms are colored in red, blue, and green, respectively. C atoms are colored in brown for the catalytic residues Asp237-His265-Cys112, gray for the substrate, and yellow for the rest of the residues. Potential hydrogen bonds are shown as dotted lines.

Table 4: Enzyme−substrate Hydrogen Bonds in the S112C + HOPDA Complex

substrate	active site residues	distance (Å)
C1-carboxylate O1	Arg190 Nη2	3.0
C1-carboxylate O1	Gly43 N	3.0
C1-carboxylate O2	Arg190 Nη1	3.0
C1-carboxylate O2	Trp266 Nϵ1	3.2
C1-carboxylate O2	Asn51 Nδ2	3.0
*C*2-carbonyl O3	His265 Nϵ2	3.3
*C*2-carbonyl O3	Asn111 Nδ2	2.9
*C*2-carbonyl O3	Trp266 Nϵ1	3.0
C6-carbonyl O4	Gly42 N	2.9
C6-carbonyl O4	Met113 N	2.8

Table 5: Conformational Flexibility of His265[a]

		distance, H265 Nϵ2 to HOPDA atoms (Å)	
structure	monomer	HOPDA C-2	HOPDA C-5
S112C + HOPDA	A	3.3	4.5
	B	3.5	3.8
S112C	A	3.9	3.5
	B	3.7	2.9
wild type	A	3.4	4.5
	B	3.8	3.1

[a] The HOPDA coordinates from the S112C + HOPDA structure were fit into the S112C and wild-type structures as described in the text.

$CumD_{IP01}$, corresponding to His265 and Trp266 in $BphD_{LB400}$, have different conformations in various CumD structures (*18*).

The potential dual role of His265 in deprotonating HOPDA at C-2 and protonating it at C-5, as suggested in MhpC (*20*, *21*), raises the issue of this residue's conformational flexibility. As described above, a clear interaction is observed between His265 and the C-2 hydroxyl/oxo of HOPDA, consistent with the role of His265 as a base. To examine the possible role of His265 in protonating C-5, the distance between C-5 and His265 Nϵ2 was measured in both subunits of the S112C + HOPDA structure. Moreover, the structures of S112C and wild type were least-square fitted to the S112C + HOPDA structure using O, and the distance between His265 and C-5 was calculated for all structures. The data (Table 5) reveal that the distance varied from 2.9 Å (deduced from subunit B of S112C) to 4.5 Å (observed in subunit A of S112C + HOPDA).

DISCUSSION

The current study provides important new insight into the mechanism of MCP hydrolases. Prior studies have provided

indirect evidence for a mechanism involving enzyme-catalyzed tautomerization of substrate to S^k, partial S^k release (*11*, *12*), and hydrolytic C−C cleavage via a *gem*-diol intermediate (Figure 2, Scheme 1) (*13*). Our single turnover stopped-flow analysis of $BphD_{LB400}$ shows the rapid formation of E:S, an intermediate having an electronic absorption maximum that is strongly red-shifted (λ_{max} = 492 nm) compared to that of the HOPDA enolate in aqueous solution (λ_{max} = 434 nm). We observed the biphasic decay of this intermediate coupled to the formation of the HPD product, with the second phase similar to k_{cat}. However, in contrast to previous work on MhpC (*11*, *12*), we were unable to detect the release of S^k, thereby precluding uncoupling as the source of the biphasic behavior. Product inhibition is consistent with HPD release prior to benzoate, and solvent viscosity did not affect k_{cat}, suggesting that benzoate may be released in a rate-determining, intramolecular step. Key active site interactions with the dienoate moiety of the substrate are observed crystallographically, suggesting that His265 may play an important role in substrate ketonization.

Nature of the Red-Shifted Intermediate. On the basis of current evidence, we cannot unequivocally identify the rapidly formed E:S species possessing the red-shifted electronic absorption maximum (492 nm). One possibility is that E:S represents an enzyme-bound HOPDA enolate. The conjugated π electron system of the enolate extends from the C-1 to C-6 carbonyls of HOPDA, and in aqueous solution absorbs maximally in the visible region at 434 nm. The red-shift observed upon binding to BphD may arise from active site interactions or a twisted conformation of the substrate. A second possibility is that E:S represents ketonized HOPDA. Ketonization disrupts the conjugated π electron system of HOPDA and, therefore, would be predicted to blue-shift the latter's spectrum. However, the enzyme active site environment may perturb the energy of this transition by polarizing the π electrons of the α,β-unsaturated keto tautomer. For example, a 90 nm red shift produced by an α,β-unsaturated thiol ester inhibitor when bound to the active site of crotonase was attributed to π electron polarization (*47*). Analogous polarization of the α,β-unsaturated moiety of ketonized HOPDA may occur in the active site of BphD. However, we expect that this red shift would have to be greater than 90 nm to compensate for the blue shift expected upon ketonization. Alternatively, the BphD-bound keto tautomer may be in equilibrium with another form of the bound substrate. Importantly, no evidence for a red-shifted species was observed when excess HPD was mixed with the enzyme, suggesting that the C5−C6 bond is intact in the absorbing species. Recent spectroscopic analyses of HOPDA bound to mutant enzymes indicate that the E:S species with the 492 nm feature possesses a ketonized HOPDA (Horsman, G. P., and Eltis, L. D., unpublished results).

Enzyme−Substrate Interactions. The S112C + HOPDA structure clearly illustrates important enzyme−substrate interactions. Previously, a hypothetical model for the $BphD_{RHA1}$−HOPDA complex (*17*) and the crystal structure of inhibitor bound to MhpC (*20*) predicted the importance of Arg190 ($BphD_{LB400}$ numbering) in anchoring the C-1 carboxylate, and the latter study also included the contribution to this function of Asn51. Our structure with the natural substrate reveals interactions of the dienoate moiety with three additional conserved residues, Asn111, His265, and Trp266. The conservation of these five residues among all known MCP hydrolases highlights their catalytic significance. Specifically, the hydrogen bonding to the C-2 oxygen demonstrates the capacity of some of these residues (Asn111, Trp266) to stabilize developing negative charge at this position during ketonization.

The ketonization reaction carried out by the MCP hydrolases is not well understood, but recent crystallographic and kinetic analyses of MhpC mutants suggested that His265 is the most likely candidate for direct transfer of a proton from the C-2 hydroxyl to C-5 (*20*, *21*). Our crystallographic observation of a hydrogen bond between His265 and the C-2 hydroxyl of the dienoate moiety significantly advances the proposed role of His265 as a general base for substrate ketonization. Although the His265 to C-5 distance is rather far in the most clearly defined density of subunit A of the S112C + HOPDA structure (4.5 Å), multiple His265 positions were observed in the various structures, including one which predicts a His265 to C-5 distance of 2.9 Å (Table 5). The flexibility in this histidine, which was also noted in structural studies of CumD (*18*), appears to be sufficient to accommodate its additional role as a general acid in the protonation of C-5. Furthermore, the native $BphD_{LB400}$-catalyzed deuterium incorporation into the H-5_E position of HPD, also seen in MhpC (*10*) and His_6-$BphD_{LB400}$ (*40*), suggests the transfer of a proton to the *proS* position of C-5 and fragmentation onto the *re* face, a stereochemical course consistent with His265-mediated proton transfer (Figure 9), rather than, for example, a general acid role for Ser112 in protonating HOPDA C-5.

Origin of Biphasic Kinetics. The biphasic behavior of E:S decay (492 nm) and HPD formation (270 nm) could not be satisfactorily explained by either the S^k release or the absorbance of a product complex. Thus, in contrast to what has been observed for another MCP hydrolase, MhpC (*11*, *12*), three independent approaches indicated that $BphD_{LB00}$ does not detectably release S^k: (1) HPD formation was apparently coupled to E:S depletion in single turnover stopped-flow experiments; (2) HPLC analysis revealed no accumulation of S^k under steady-state conditions; and (3) the levels of nonspecific deuterium incorporation into HPD were low. Other explanations for the biphasic kinetics must, therefore, be explored.

We considered two models to account for the biphasic decay. In the E:S^e model (Scheme 2), the absorbing species in E:S (λ_{max} = 492 nm) is the HOPDA enolate. Moreover, $1/\tau_1$, $1/\tau_2$, and $1/\tau_3$ reflect deprotonation (or twisting of the enolate), ketonization, and C−C cleavage, respectively. The biphasic decay of E:S^e at the observed values for $1/\tau_2$ and $1/\tau_3$ can be appropriately modeled (*48*)[4] assuming that ketonization is a reversible process with approximately equal forward and reverse rate constants ($k_2 \approx k_{-2} \approx 20\ s^{-1}$) and that the subsequent C−C cleavage is irreversible ($k_3 \approx 15\ s^{-1}$). However, this model is inconsistent with several experimental observations. First, $1/\tau_2$ decreased with increased solvent viscosity. This is not consistent with an intramolecular event such as ketonization, which should not be affected by viscosity. Second, we obtained no spectroscopic evidence of a ketonized intermediate, that

[4] $1/\tau_2 = (p + q)/2$; $1/\tau_3 = (p - q)/2$; where $p = k_2 + k_{-2} + k_3 + k_{-3}$; and $q = [p^2 - 4(k_2k_3 + k_{-2}k_{-3} + k_2k_{-3})]^{1/2}$ (*48*).

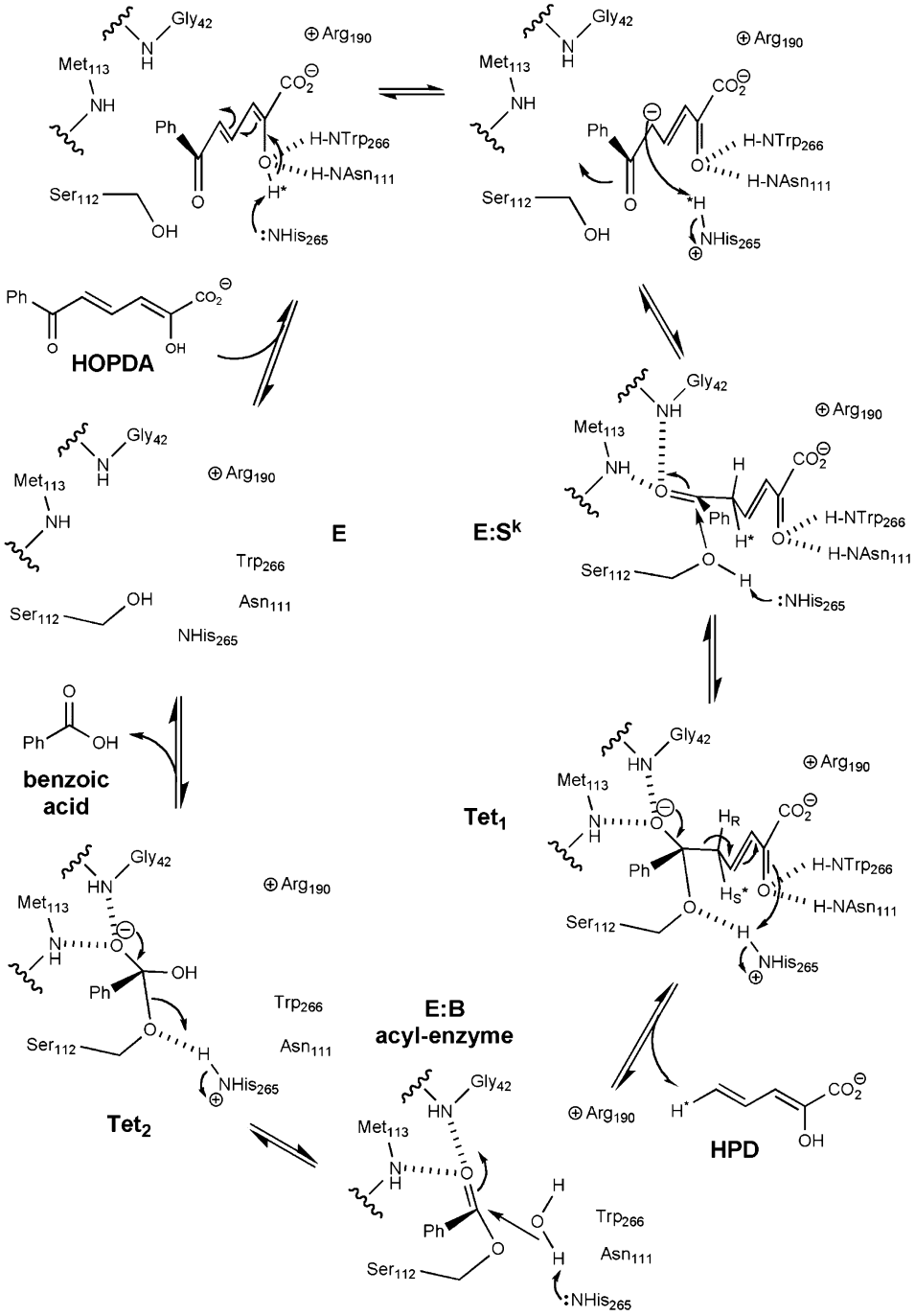

FIGURE 9: Possible mechanism of $BphD_{LB400}$. The free enzyme (E) binds and ketonizes HOPDA via a His265-catalyzed transfer of a proton (H*) to the *proS* position at C-5, generating $E:S^k$. Nucleophilic attack on $E:S^k$ generates the first tetrahedral intermediate (Tet_1), the negative charge of which is stabilized by the main chain amide protons of the oxyanion hole residues, Met113 and Gly42. The collapse of Tet_1 involves C−C fragmentation onto the *re* face of the double bond, generating the acyl−enzyme intermediate (E:B) and releasing HPD with the inserted proton at the H-5_E position. His265 activates water to attack at the acyl−enzyme carbonyl, generating the second tetrahedral intermediate (Tet_2), the collapse of which releases benzoate and regenerates the free enzyme. For clarity, the conserved residues Asp237 (of the catalytic triad) and Asn51 (interacts with the HOPDA carboxylate) are omitted.

Scheme 2

$$E + S \overset{K_S}{\rightleftharpoons} \underset{(492\ nm)}{E:S^e} \underset{k_{-2} \sim 20\ s^{-1}}{\overset{k_2 \sim 20\ s^{-1}}{\rightleftharpoons}} E:S^k \xrightarrow[H_2O]{k_3 \sim 15\ s^{-1}} E + H + B$$

is, the appearance of the species that absorbs maximally at 270 nm is apparently coupled to the decay of E:S. For this to be true in the $E:S^e$ model, HPD and ketonized HOPDA would have to possess essentially identical spectra, including similar molar absorptivities at 270 nm. This seems unlikely considering that the enol tautomer of HPD (analogous to enol-HOPDA) absorbs maximally at 270 nm, whereas the keto tautomer (analogous to keto-HOPDA) does not. Finally, this model does not readily explain the apparent ordered release of products suggested from product inhibition experiments.

In the two-conformation model (Scheme 3), $1/\tau_1$ reflects ketonization and the biphasic kinetics result from two interconverting enzyme conformations: E, capable of cata-

Scheme 3

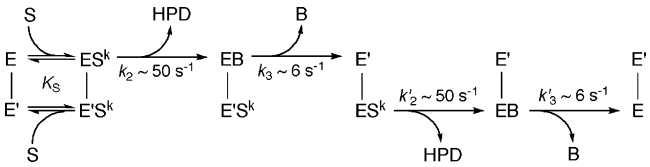

lyzing C−C cleavage/HPD release, and E′, incapable of C−C cleavage/HPD release. C−C cleavage/HPD dissociation (k_2) and benzoate release (k_3) must occur in E (half the enzyme sites) before a conformational change converts E′ (the other half of the active sites) to E, thereby allowing catalysis to proceed in the remaining active sites. Hence, each subunit cycles between E and E′ conformations.

Several lines of evidence are consistent with a two-conformation model. First, the amplitudes of $1/\tau_2$ and $1/\tau_3$ were approximately equal to each other under all experimental conditions investigated herein, suggesting that they represent events occurring in 50% of the enzyme molecules. Second, increased solvent viscosity, achieved by adding glycerol, decreased $1/\tau_2$ but has no effect on $1/\tau_3$. According to Scheme 3, $1/\tau_2$ represents C−C cleavage/HPD release in 50% of the enzyme molecules and should, thus, be sensitive to the effect of viscosity on diffusive HPD release occurring with the rate constant k_2. In contrast, $1/\tau_3$ is unaffected by viscosity, consistent with the proposal that this relaxation contains contributions from a rate-limiting (because $1/\tau_3 \approx k_{cat}$), nondiffusive release of benzoate (k_3), followed by rapid HPD formation in the remaining half sites (k_2'). Third, this model more reasonably assigns the absorbance at 270 nm solely to HPD and does not require an equivalent molar absorptivity of ketonized HOPDA. Fourth, the observed ordered product release is accounted for in this scenario. Finally, significant conformational differences are observed between the active sites of monomers A and B in several of the crystal structures, and in the S112C + HOPDA structure, the density for the substrate is less clear in monomer B than in monomer A, suggesting lower occupancy.

The two-conformation model is intriguing in light of crystallographic evidence. First, in an MhpC−inhibitor complex, the substrate analogue was bound to only one subunit of the dimer (*20*). Moreover, openings to the subsites in the MhpC structures are of insufficient diameter to permit the passage of substrate, suggesting that some movement is necessary for substrate binding and product release (*20*). However, single turnover stopped-flow analysis of MhpC at neutral pH exhibited only a single relaxation assigned to the C−C cleavage/product release (*21*), suggesting that the apparent half-of-sites reactivity does not influence this step. Stopped-flow analysis of HOPDA hydrolysis by His_6-$BphD_{LB400}$ also demonstrated a single-step kinetic mechanism for substrate disappearance and HPD formation (*40*). However, it is possible that the histidine tag disrupts the quaternary structure that gives rise to the two distinct enzyme conformers.

Structural data further suggest at least two origins of a conformational change: the lid domain and Arg190. Thus, some conformational differences in the lid domains occur among our structures. Movement in the lid domain could be analogous to what occurs in other α/β-hydrolases such as lipases (*7*, *8*). In BphD, the lid domains make contacts dependent on the tetramer (i.e., the AB′ dimer in Figure 6). Consistent with an apparent single step for product release in MhpC, the MhpC dimer corresponds to the AB dimer of BphD, in which the lid domains do not interact directly with each other (*20*). Alternatively, the conformational change could involve movement of Arg190 to facilitate HPD release. This residue is directed toward the solvent in some MCP hydrolase crystal structures, greatly increasing the solvent accessibility of the P subsite (*17*, *18*). It is possible that conformational changes in the lid domain movement and Arg190 occur in a concerted manner to facilitate HPD release.

Possibility of an Acyl-Enzyme Intermediate. A notable feature of the results is that k_3 is both rate-determining *and* unaffected by viscosity. In the two-conformation model, two mechanisms may be invoked to explain k_3: (1) the conformational change accompanying the release of benzoate is rate-limiting or (2) the conformational change occurs rapidly after a rate-limiting hydrolysis of a benzoyl−enzyme intermediate. Consideration of the product inhibition data in light of the structural data is most consistent with the second mechanism. Thus, in all three $BphD_{LB400}$ structures, the benzoate-binding (NP) subsite of the active site is freely accessible to the solvent whereas the HPD-binding (P) subsite appears to be partially occluded. Hence, in the absence of a covalent intermediate (e.g., the *gem*-diol mechanism, Figure 2), the structural data indicate that benzoate should be released first. However, the product inhibition data suggest that HPD is released from the enzyme prior to benzoate. The apparent contradiction between the product inhibition and structural data may be reconciled by invoking a conformational change.

A simpler explanation for the observed ordered release of products is that catalysis involves a more conventional role for the catalytic serine whereby it attacks S^k to liberate HPD, and the remaining covalent benzoyl−enzyme complex is hydrolyzed in a final, rate-determining step (Figure 9). Such a nucleophilic mechanism is consistent with the viscosity effects outlined above. Moreover, the crystallographic observation of a hemi-ketal adduct in the MhpC−inhibitor complex (*20*) demonstrates that the catalytic serine is capable of nucleophilic attack at a substrate carbonyl. In light of the uncertain role of the catalytic serine in MCP hydrolases, we are performing experiments using BphD to distinguish mechanisms involving *gem*-diol and acyl−enzyme intermediates.

ACKNOWLEDGMENT

We thank Yong Ge for purified C23O, Fred Vaillancourt for purified DHBD, Mark Okon for assistance in acquiring NMR spectra, Shouming He for the mass spectrometric analysis, Cheryl Whiting for technical assistance, and Martin Tanner for reading the manuscript. Use of the Argonne National Laboratory Structural Biology Center and BioCARS beamlines at the Advanced Photon Source was supported by the U.S. Department of Energy, Office of Biological and Environmental Research, under Contract No. W-31-109-ENG-38. We are grateful to the staff of both sectors. Use of the BioCARS Sector 14 was also supported by the National Institutes of Health, National Center for Research Resources, under grant number RR07707.

REFERENCES

1. Dagley, S. (1975) A biochemical approach to some problems of environmental pollution, *Essays Biochem. 11*, 81−138.
2. Pieper, D. H. (2005) Aerobic degradation of polychlorinated biphenyls, *Appl. Microbiol. Biotechnol. 67*, 170−191.
3. Seah, S. Y. K., Labbé, G., Nerdinger, S., Johnson, M. R., Snieckus, V., and Eltis, L. D. (2000) Identification of a serine hydrolase as a key determinant in the microbial degradation of polychlorinated biphenyls, *J. Biol. Chem. 275*, 15701−15708.
4. Ohtsubo, Y., Kudo, T., Tsuda, M., and Nagata, Y. (2004) Strategies for bioremediation of polychlorinated biphenyls, *Appl. Microbiol. Biotechnol. 65*, 250−258.
5. Rengarajan, J., Bloom, B. R., and Rubin, E. J. (2005) Genome-wide requirements for *Mycobacterium tuberculosis* adaptation and survival in macrophages, *Proc. Natl. Acad. Sci. U.S.A. 102*, 8327−8332.
6. Anderton, M. C., Bhakta, S., Besra, G. S., Jeavons, P., Eltis, L. D., and Sim, E. (2006) Characterization of the putative operon containing arylamine *N*-acetyltransferase (*nat*) in *Mycobacterium bovis* BCG, *Mol. Microbiol. 59*, 181−192.
7. Ollis, D. L., Cheah, E., Cygler, M., Dijkstra, B., Frolow, F., Franken, S. M., Harel, M., Remington, S. J., Silman, I., Schrag, J., Sussman, J. L., Verscheuren, K. H. G., and Goldman, A. (1992) The alpha/beta hydrolase fold, *Protein Eng. 5*, 197−211.
8. Holmquist, M. (2000) Alpha/beta hydrolase fold enzymes: Structures, functions and mechanisms, *Curr. Protein Pept. Sci. 1*, 209−235.
9. Heikinheimo, P., Goldman, A., Jeffries, C., and Ollis, D. L. (1999) Of barn owls and bankers: A lush variety of alpha/beta hydrolases, *Structure 7*, 141−146.
10. Lam, W. W. Y., and Bugg, T. D. H. (1994) Chemistry of extradiol aromatic ring cleavage: Isolation of a stable dienol ring fission intermediate and stereochemistry of its enzymatic hydrolytic cleavage, *J. Chem. Soc., Chem. Commun.*, 1163−1164.
11. Lam, W. W. Y., and Bugg, T. D. H. (1997) Purification, characterization, and stereochemical analysis of a C-C hydrolase: 2-Hydroxy-6-keto-nona-2, 4-diene-1, 9-dioic acid 5, 6-hydrolase, *Biochemistry 36*, 12242−12251.
12. Henderson, I. M. J., and Bugg, T. D. H. (1997) Pre-steady-state kinetic analysis of 2-hydroxy-6-keto-nona-2, 4-diene-1, 9-dioic acid 5, 6-hydrolase: Kinetic evidence for enol/keto tautomerization, *Biochemistry 36*, 12252−12258.
13. Fleming, S. M., Robertson, T. A., Langley, G. J., and Bugg, T. D. H. (2000) Catalytic mechanism of a C-C hydrolase enzyme: Evidence for a *gem*-diol intermediate, not an acyl enzyme, *Biochemistry 39*, 1522−1531.
14. Speare, D. M., Fleming, S. M., Beckett, M. N., Li, J. J., and Bugg, T. D. H. (2004) Synthetic 6-aryl-2-hydroxy-6-ketohexa-2, 4-dienoic acid substrates for C-C hydrolase BphD: Investigation of a general base catalytic mechanism, *Org. Biomol. Chem. 2*, 2942−2950.
15. Speare, D. M., Olf, P., and Bugg, T. D. H. (2002) Hammett analysis of a C-C hydrolase-catalysed reaction using synthetic 6-aryl-2-hydroxy-6-ketohexa-2, 4-dienoic acid substrates, *Chem. Commun. (Cambridge, U.K.)*, 2304−2305.
16. Bugg, T. D. H. (2004) Diverse catalytic activities in the alpha beta-hydrolase family of enzymes: Activation of H_2O, HCN, H_2O_2, and O_2, *Bioorg. Chem. 32*, 367−375.
17. Nandhagopal, N., Yamada, A., Hatta, T., Masai, E., Fukuda, M., Mitsui, Y., and Senda, T. (2001) Crystal structure of 2-hydroxyl-6-oxo-6-phenylhexa-2, 4-dienoic acid (HPDA) hydrolase (BphD enzyme) from the Rhodococcus sp. strain RHA1 of the PCB degradation pathway, *J. Mol. Biol. 309*, 1139−1151.
18. Fushinobu, S., Saku, T., Hidaka, M., Jun, S. Y., Nojiri, H., Yamane, H., Shoun, H., Omori, T., and Wakagi, T. (2002) Crystal structures of a meta-cleavage product hydrolase from *Pseudomonas fluorescens* IP01 (CumD) complexed with cleavage products, *Protein Sci. 11*, 2184−2195.
19. Habe, H., Morii, K., Fushinobu, S., Nam, J. W., Ayabe, Y., Yoshida, T., Wakagi, T., Yamane, H., Nojiri, H., and Omori, T. (2003) Crystal structure of a histidine-tagged serine hydrolase involved in the carbazole degradation (CarC enzyme), *Biochem. Biophys. Res. Commun. 303*, 631−639.
20. Dunn, G., Montgomery, M. G., Mohammed, F., Coker, A., Cooper, J. B., Robertson, T., Garcia, J. L., Bugg, T. D. H., and Wood, S. P. (2005) The structure of the C-C bond hydrolase MhpC provides insights into its catalytic mechanism, *J. Mol. Biol. 346*, 253−265.
21. Li, C., Montgomery, M. G., Mohammed, F., Li, J. J., Wood, S. P., and Bugg, T. D. H. (2005) Catalytic mechanism of C-C hydrolase MhpC from *Escherichia coli*: Kinetic analysis of His263 and Ser110 site-directed mutants, *J. Mol. Biol. 346*, 241−251.
22. Nerdinger, S., Kendall, C., Marchhart, R., Riebel, P., Johnson, M. R., Yin, C. F., Eltis, L. D., and Snieckus, V. (1999) Directed ortho metalation and Suzuki-Miyaura cross-coupling connections: Regiospecific synthesis of all isomeric chlorodihydroxybiphenyls for microbial degradation studies of PCBs, *Chem. Commun. (Cambridge, U.K.)*, 2259−2260.
23. Seah, S. Y. K., Terracina, G., Bolin, J. T., Riebel, P., Snieckus, V., and Eltis, L. D. (1998) Purification and preliminary characterization of a serine hydrolase involved in the microbial degradation of polychlorinated biphenyls, *J. Biol. Chem. 273*, 22943−22949.
24. Seah, S. Y., Terracina, G., Bolin, J. T., Riebel, P., Snieckus, V., and Eltis, L. D. (1998) Purification and preliminary characterization of a serine hydrolase involved in the microbial degradation of polychlorinated biphenyls, *J. Biol. Chem. 273*, 22943−22949.
25. Doublié, S. (1997) Preparation of selenomethionyl proteins for phase determination, *Methods Enzymol. 276*, 523−530.
26. Cornish-Bowden, A. (1995) *Analysis of Enzyme Kinetic Data*, Oxford University Press, New York.
27. Lian, H. L., and Whitman, C. P. (1993) Ketonization of 2-hydroxy-2, 4-pentadienoate by 4-oxalocrotonate tautomerase: Implications for the stereochemical course and the mechanism, *J. Am. Chem. Soc. 115*, 7978−7984.
28. McPherson, A. (1982) *The Preparation and Analysis of Protein Crystals*, John Wiley & Sons, New York.
29. Otwinowski, Z., and Minor, W. (1997) Processing of X-ray diffraction data collected in oscillation mode, *Methods Enzymol. 276*, 307−326.
30. O'Neill, P., Stevens, D. L., and Garman, E. F. (2002) Physical and chemical considerations of damage induced in protein crystals by synchrotron radiation: A radiation chemical perspective, *J. Synchrotron Radiat. 9*, 329−332.
31. Terwilliger, T. C., and Berendzen, J. (1999) Automated MAD and MIR structure solution, *Acta Crystallogr., Sect. D 55*, 849−861.
32. Bailey, S. (1994) The *CCP*4 suite: Programs for protein crystallography, *Acta Crystallogr., Sect. D 50*, 760−763.
33. Jones, T. A., Zou, J. Y., Cowan, S. W., and Kjeldgaard, M. (1991) Improved methods for building protein models in electron density maps and the location of errors in these models, *Acta Crystallogr., Sect. A 47*, 110−119.
34. Brunger, A. T., Adams, P. D., Clore, G. M., DeLano, W. L., Gros, P., Grosse-Kunstleve, R. W., Jiang, J. S., Kuszewski, J., Nilges, M., Pannu, N. S., Read, R. J., Rice, L. M., Simonson, T., and Warren, G. L. (1998) Crystallography & NMR system: A new software suite for macromolecular structure determination, *Acta Crystallogr., Sect. D 54*, 905−921.
35. Seah, S. Y. K., Labbé, G., Kaschabek, S. R., Reifenrath, F., Reineke, W., and Eltis, L. D. (2001) Comparative specificities of two evolutionarily divergent hydrolases involved in microbial degradation of polychlorinated biphenyls, *J. Bacteriol. 183*, 1511−1516.
36. Hiromi, K. (1979) *Kinetics of Fast Enzyme Reactions*, Halsted Press, Tokyo, Japan.
37. Pollard, J. R., Henderson, I. M. J., and Bugg, T. D. H. (1997) Chemical and biochemical properties of 2-hydroxypentadienoic acid, a homologue of enolpyruvic acid, *Chem. Commun. (Cambridge, U.K.)*, 1885−1886.
38. Adams, J. A., and Taylor, S. S. (1992) Energetic limits of phosphotransfer in the catalytic subunit of cAMP-dependent protein kinase as measured by viscosity experiments, *Biochemistry 31*, 8516−8522.
39. Cole, P. A., Burn, P., Takacs, B., and Walsh, C. T. (1994) Evaluation of the catalytic mechanism of recombinant human Csk (C-terminal Src kinase) using nucleotide analogs and viscosity effects, *J. Biol. Chem. 269*, 30880−30887.
40. Li, J. J., and Bugg, T. D. H. (2005) Stereochemistry of the reaction catalysed by 2-hydroxy-6-keto-6-phenyl-hexa-2, 4-dienoic acid 5, 6-hydrolase (BphD), *Chem. Commun. (Cambridge, U.K.)*, 130−132.

41. Whitman, C. P., Aird, B. A., Gillespie, W. R., and Stolowich, N. J. (1991) Chemical and enzymatic ketonization of 2-hydroxymuconate, a conjugated enol, *J. Am. Chem. Soc. 113*, 3154−3162.
42. Cornish-Bowden, A. (2004) *Fundamentals of Enzyme Kinetics*, 3rd ed., Portland Press, London.
43. Nicholls, A., Sharp, K. A., and Honig, B. (1991) Protein folding and association: Insights from the interfacial and thermodynamic properties of hydrocarbons, *Proteins: Struct., Funct., Genet. 11*, 281−296.
44. Jocelyn, P. C. (1972) *Biochemistry of the SH Group*, Academic Press, London.
45. Pathak, D., and Ollis, D. (1990) Refined structure of dienelactone hydrolase at 1.8 Å, *J. Mol. Biol. 214*, 497−525.
46. Kamphuis, I. G., Kalk, K. H., Swarte, M. B., and Drenth, J. (1984) Structure of papain refined at 1.65 Å resolution, *J. Mol. Biol. 179*, 233−256.
47. D'Ordine, R. L., Tonge, P. J., Carey, P. R., and Anderson, V. E. (1994) Electronic rearrangement induced by substrate-analog binding to the enoyl-CoA hydratase active site: Evidence for substrate activation, *Biochemistry 33*, 12635−12643.
48. Fersht, A. (1999) *Structure and Mechanism in Protein Science*: *A Guide to Enzyme Catalysis and Protein Folding*, W. H. Freeman, New York.

BI0611098